ACS OMEGA

http://pubs.acs.org/journal/acsodf

Article

The Impact of the Serum Extraction Protocol on Metabolomic Profiling Using UPLC-MS/MS and FTIR Spectroscopy

Tiago A. H. Fonseca, Cristiana P. Von Rekowski, Rúben Araújo, M. Conceição Oliveira, Gonçalo C. Justino, Luís Bento, and Cecília R. C. Calado*

Cite This: *ACS Omega* 2023, 8, 20755−20766

Read Online

ACCESS | Metrics & More | Article Recommendations | Supporting Information

ABSTRACT: Biofluid metabolomics is a very appealing tool to increase the knowledge associated with pathophysiological mechanisms leading to better and new therapies and biomarkers for disease diagnosis and prognosis. However, due to the complex process of metabolome analysis, including the metabolome isolation method and the platform used to analyze it, there are diverse factors that affect metabolomics output. In the present work, the impact of two protocols to extract the serum metabolome, one using methanol and another using a mixture of methanol, acetonitrile, and water, was evaluated. The metabolome was analyzed by ultraperformance liquid chromatography associated with tandem mass spectrometry (UPLC-MS/MS), based on reverse-phase and hydrophobic chromatographic separations, and Fourier transform infrared (FTIR) spectroscopy. The two extraction protocols of the metabolome were compared over the analytical platforms (UPLC-MS/MS and FTIR spectroscopy) concerning the number of features, the type of features, common features, and the reproducibility of extraction replicas and analytical replicas. The ability of the extraction protocols to predict the survivability of critically ill patients hospitalized at an intensive care unit was also evaluated. The FTIR spectroscopy platform was compared to the UPLC-MS/MS platform and, despite not identifying metabolites and consequently not contributing as much as UPLC-MS/MS in terms of information concerning metabolic information, it enabled the comparison of the two extraction protocols as well as the development of very good predictive models of patient's survivability, such as the UPLC-MS/MS platform. Furthermore, FTIR spectroscopy is based on much simpler procedures and is rapid, economic, and applicable in the high-throughput mode, i.e., enabling the simultaneous analysis of hundreds of samples in the microliter range in a couple of hours. Therefore, FTIR spectroscopy represents a very interesting complementary technique not only to optimize processes as the metabolome isolation but also for obtaining biomarkers such as those for disease prognosis.

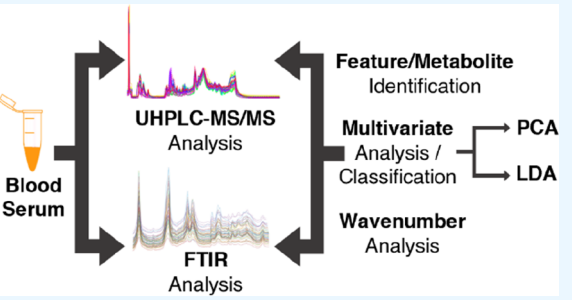

INTRODUCTION

Metabolomics is placed at the downstream of genomics, transcriptomics, and proteomics[1−3] and consequently reflects directly the organism's status and dynamic responses to disturbances from genetic and environmental factors, including diseases, microbiota, diet, stress, gender, age, and lifestyle, among others.[1,2] Metabolomics includes the profiling of small-dimension compounds (e.g., sugars, amino acids, peptides, lipids, and others below 1.5 kDa) and the understanding of the metabolite's interaction, mechanisms of action, and functions, i.e., the metabolic pathway network. According to The Human Metabolome Database (HMDB), there are over 250 000 total metabolites present in the human body.[4] If the goal is to discover a biomarker for the diagnosis and prognosis of a disease, usually the metabolome from a biofluid, as serum, is determined. Biofluid analysis, including serum and plasma or urine, presents advantages of being obtained by noninvasive or minimally invasive methods while reflecting the pathophysiological state of the organism.[5] Therefore, biofluid metabolomics can be used as a starting step toward personalized medicine[6] by enabling the prediction of diseases' biomarkers, such as for Parkinson's disease,[7] type 2 diabetes,[8] and the prediction of transplant rejection,[9] among others.

There are diverse and complementary analytical techniques to retrieve the system's metabolome,[10] one of the most common approaches being based on ultraperformance liquid chromatography coupled to tandem mass spectrometry (UPLC-MS/MS) due to the wide metabolite coverage offered by the wide-ranging selectivity in LC separation and great sensitivity in MS/MS detection. The dynamic range of these analytical setups enables the acquisition of data over 3−5 orders of magnitude and the detection of metabolite concentrations less than 0.01% from the highest metabolite

Received: February 28, 2023
Accepted: May 4, 2023
Published: June 1, 2023

intensity.[11] Depending on the characteristics of the LC separation system, different molecules can be highlighted. For example, from the most common LC techniques used, hydrophilic interaction liquid chromatography (HILIC), detects mostly polar molecules, where reverse-phase (RP) separation focuses on non- to midpolar compounds.[12]

Fourier transform infrared (FTIR) spectroscopy is a technique used to acquire the metabolic profile of a biosystem with high sensitivity and specificity.[13−16] The technique may be used to quantitatively determine the concentration of target metabolites[14] but is generally applied to define the system's metabolic status in a more holistic mode by relating the spectra or spectral bands via multivariate data analysis, including machine learning techniques, to a specific phenotype, i.e., to a pathophysiological state.[13,15] A high advantage of this technique approach is the high-throughput capacity in analyzing hundreds to thousands of samples at once in a rapid, simple, and economic way while enabling the development of highly accurate, sensitive, and specific models to predict the target's phenotype.[13,16] Based on these last characteristics, and despite the technique not enabling the acquisition of detailed information concerning the system metabolome, it can be applied to conduct a qualitative evaluation of sample preparation for metabolomics, as conducted by Kuligowski et al., for example.[17]

The sample processing method used to isolate the metabolome is also critical, since it will affect the type of metabolites that will be obtained and the reproducibility of the process. Unfortunately, there are no standard operating procedures to prepare biological samples before the metabolome analysis. The preparation of human biofluids usually includes one step to remove macromolecules. In the case of plasma, serum, and urine, several methods to precipitate macromolecules can be used, e.g., based on organic solvents, salts, or changes in pH. Solid-phase extraction, hybrid platforms, or microextractions[18] are usually time-consuming and costly when considering large cohorts. Salts may affect the chromatographic separation, while low pH can adversely affect some compounds' stability. For example, Want et al.[19] compared diverse methods to extract the serum metabolome, subsequently analyzed by LC-MS/MS, ranging from organic solvents and acids to heat denaturation. Methanol precipitation was the most effective, straightforward, and reproducible approach, covering 2000 detected features. The methanol-based method also achieved the highest protein removal (98%), which may positively influence the lifetime of chromatographic columns while minimizing the contamination of the electrospray interface.

For all of the above, most authors use an organic solvent or a solvent mixture to precipitate high-dimension molecules, followed by a centrifugation step to separate the precipitate from the metabolite-containing supernatant. This step is usually described as deproteinization, despite other macromolecules also being eliminated, or metabolome extraction. A frequent procedure in this step makes use of 80% methanol, which leads to the detection of a large number of amphiphilic metabolites with mixed polarity.[20,21] For example, based on an experimental design to evaluate the efficiency of five organic solvents (methanol, ethanol, acetonitrile, acetone, and chloroform), singly or in combination, in the extraction of the metabolome from plasma through GC-MS, A et al.[22] observed that methanol extraction, at 80% (v/v), was the most efficient and reproducible method. This was corroborated by Want et al.[19] when detecting 2056 features in the serum metabolome extracted with methanol and analyzed by LC-MS/MS, in comparison to 1606 features obtained with acetonitrile. The methanol-based extraction led to the most precise analysis (general standard deviation of 25%), whereas the worst performing analysis was obtained with acetonitrile (36%).

Due to the relevance of sample processing procedures, the present work aims to evaluate the effect of the metabolome extraction protocol on serum samples from coronavirus disease 2019 (COVID-19) patients based on a methanol extraction process and on a mixture of acetonitrile, methanol, and water, since acetonitrile can lead to the extraction of more polar metabolites.[17] The impact of the extraction process was evaluated by UPLC-MS/MS, performed on RP and HILIC systems, and by FTIR-spectroscopy. The capacity of both extraction methods to predict patient survivability during hospitalization at an intensive care unit (ICU) was also evaluated. Due to the more economic and high-throughput capabilities of FTIR-spectroscopy, this technique was compared to the UPLC-MS/MS platform in terms of data reproducibility and the capacity to predict the patients' outcomes.

METHODS

Patients. Serum samples from six male patients diagnosed with COVID-19 by RT-PCR assay (demographic data given in Table S1) were obtained from peripheral whole blood, by centrifugation at 3000 rpm for 10 min, from COVID-19 patients admitted to the ICU of Hospital São José, Centro Hospitalar Universitário Lisboa Central according to legal requirements, including project ethics approval by the Hospital Ethics Committee.

Serum Sample Preparation. Serum samples were kept at −80 °C until extraction. During the metabolome extraction, samples were kept on ice. Solvents were kept at −80 °C (Optima LC/MS grade, Fisher Chemical). The metabolome was obtained by mixing 75 μL of serum with 265 μL of solvent according to Roberts et al.[23] Two extraction protocols were conducted per sample, where in one protocol the solvent was only methanol and in the second protocol a mixture of methanol, acetonitrile, and water at 2:2:1 (v/v) according to Lu et al.[24] was used. After solvent addition, samples were vortexed and subsequently centrifuged at 18 000 × *g* for 15 min at 4 °C (Mixtasel, J.P. Selecta). The samples' supernatants were collected and stored at −80 °C until analysis. For each extraction protocol, each sample was extracted in triplicate.

Each extraction triplicate was subsequently analyzed in quadruplicate by FTIR-spectroscopy. Therefore, for each sample, a total of 12 FTIR spectra were considered.

Each extraction duplicate was subsequently analyzed in triplicate by UPLC-MS/MS. Therefore, for each sample, a total of six analyses by UPLC-MS/MS were considered. Due to sample limitations, for one of the extraction replicas of two patients' samples, only a unique and duplicate extraction analysis was conducted, respectively.

UPLC-MS/MS. Each sample was analyzed, if not otherwise stated, in triplicate by a UPLC (Bruker Daltonics GmbH) system coupled to a QqTOF Impact II mass spectrometer through an electrospray ion source (Bruker Daltonics GmbH & Co.). Samples were analyzed by two chromatographic modes, RP and HILIC. The RP system was based on a Luna 2.5 μm C18(2)-HST column (100 Å, 150 × 2 mm, Phenomenex) at a constant temperature of 40 °C, and a

https://doi.org/10.1021/acsomega.3c01370
ACS Omega 2023, 8, 20755−20766

gradient elution was used at a flow rate of 250 μL/min as follows (mobile phase A, 0.1% formic acid in water; mobile phase B, 0.1% formic acid in acetonitrile): 0.0−0.5 min 0% B, 0.5−1.5 min 0−20% B, 1.5−4.0 min 20−60% B, 4.0−6.0 min 60−100% B, 6.0−9.0 min 100% B, 9.0−10.0 min 100−0% B, and 10.0−15.0 min 0% B. For HILIC separations, a XBridge BEH Amide XP column (130 Å, 2.5 μm, 150 × 2.1 mm, Waters) was used at a constant temperature of 40 °C. With a flow rate of 250 μL/min, a gradient elution of 10 mM ammonium acetate in water containing 0.1% acetic acid (A) and 10 mM ammonium acetate in acetonitrile containing 2% water and 0.1% acetic acid (B) was applied as follows: 0−2 min 90% B, 2−6 min 90−70% B, 6−9 min 70−30% B, 9−13 min 30% B, 13−18 min 30−90% B, 18−22 min 90% B.

MS acquisition parameters were set as follows: capillary voltage of 3 kV (ESI−) or 4.5 kV (ESI+), end plate offset of 500 V, nebulizer of 4.0 bar, dry gas flow of 8.0 L/min, and dry heater temperature of 200 °C. Spectral acquisition was performed with an absolute threshold of 25 counts per 1000. For auto MS/MS data acquisition, the capillary voltage was set at 4.5 (ESI+) or 3.5 kV (ESI−) with an end plate offset of 500 V, a nebulizer pressure of 4.0 bar, a dry gas flow of 8.0 L/min, and a heater temperature of 200 °C. Spectra. acquisition was performed with a threshold of 20 counts per 1000, a cycle time of 3.0 s with exclusion after 3 spectra, and release after 1.00 min. Internal calibration was achieved with a sodium formate/acetate solution introduced to the ion source via a 20 μL loop at the beginning of each analysis. Calibration was then performed using high-precision calibration mode (HPC). All acquisitions were performed with a m/z range from 50 to 1300 with a 3 Hz spectra rate. Three full scans and one auto MS/MS scan were performed for each sample using both positive and negative ionization mode. A 25 μM solution containing quercetin, L-tryptophan (indole-d5), L-valine (d8), sulfolene (d4), and *N*,*N*-dimethyl-d6 glycine HCl was prepared and used as quality control. This QC sample was analyzed every 6 h to ensure that chromatographic resolution and spectrometer detection did not change throughout time.

Acquired MS data were preprocessed using Data Analysis (versions 4.1, 4.4, and 4.5, Bruker Daltoniks), converted to mzXML using ProteoWizard MSConvert[25], and uploaded to the XCMS server,[26−29] where data processing (including feature detection, retention time correction, peak alignment, and METLIN annotation), pairwise sample comparison, multimodal analysis (independent of separation and acquisition modes), and global metanalysis were performed. XCMS parameters fitted for the instrumental setup are given in Table S2. XCMS metabolite identification was confirmed by analyzing the MS/MS fragmentation pattern for the metabolites discussed. Principal component analysis (PCA) and linear discriminant analysis (LDA) of UPLC-MS/MS data were conducted on The Unscrambler X, version 10.5 (CAMO software AS, version 10.4, Oslo, Norway).

FTIR Spectroscopy. Each sample was analyzed in quadruplicate. Five microliters of each sample were plated in a 384-well silicon microplate (Bruker Optics GmbH & Co. KG) and then placed on a desiccator under vacuum for 2.5 h. Spectra were acquired with an FTIR spectrometer (Vertex 70, Bruker Optics GmbH & Co. KG) associated with an HTS-XT system (Bruker Optics GmbH & Co. KG). Each spectrum resulted from 64 scans with a 2 cm^{-1} resolution between 400 and 4000 cm^{-1}. The first well of the microplate was kept empty and its spectrum was used as background, according to the HTS-XT manufacturer instructions. Spectra were preprocessed by atmospheric correction and baseline corrections with OPUS software (version 6.5, Bruker Optics GmbH & Co. KG). Spectral normalization and spectral PCA and PCA-LDA were conducted on The Unscrambler X, version 10.5 (CAMO software AS, version 10.4, Oslo, Norway). PCA-LDA was conducted after outlier removal according to PCA's influence plot.

Other Statistical Analyses. For the reproducibility analysis, continuous variables (spectral bands and m/z intensities) were expressed as the median and interquartile range (25th percentile and 75th percentile). The normality of the continuous variables was tested with the Kolmogorov−Smirnov test with the Lilliefors correction. Comparison between groups was performed using the Mann−Whitney U Test, since normality was not verified. Multidimensional scaling (MDS) was based on Euclidean distance of FTIR spectral bands or m/z intensities.

For analysis of metabolites between deceased and surviving patients, a Student's t test pairwise comparison was performed between deceased and survivor patients at $p < 0.05$. All analyses were conducted on IBM SPSS Statistics version 26.

RESULTS

Two extraction protocols were applied to obtain the serum metabolome, where in one protocol only methanol (MeOH) was used and on the second protocol a mixture of acetonitrile (ACN), MeOH, and water was used. For simplicity, the protocol with a mixture of solvents will be referred to as ACN/MeOH. The metabolome was subsequently analyzed by UPLC-MS/MS and FTIR-spectroscopy. The effect of the extraction protocol was evaluated based on the following:

- Features obtained from UPLC-MS/MS and FTIR spectroscopy, such as m/z, retention time, and molecular fingerprint, respectively.
- The reproducibility concerning extraction replicas and analytical replicas.
- The development of predictive models of patient survivability.

Characteristic Features. For the UPLC-MS/MS-based system, data obtained from both RP and HILIC columns from four patients' samples (highlighted in bold in Table S1) were considered. The number of features (i.e., m/z peaks per retention time) acquired along the UPLC-MS/MS platform by the two extraction protocols are highlighted in Table 1. It was observed that the RP-based system led to between 4.2- and 5-fold more features in comparison to the HILIC, according to other authors.[30,31] However, other authors indicated the opposite.[5,32] These inconsistencies may be caused by differ-

Table 1. Molecular Features (i.e., m/z Peaks) Detected by UPLC-MS/MS Using RP and HILIC Systems from the Two Extraction Protocols

HPLC column	MeOH	ACN/MeOH	distinct features[a]
RP positive mode	1198	1402	742
RP negative mode	325	283	104
HILIC positive mode	6	5	
HILIC negative mode	353	332	79

[a]Number of features in mean terms significantly different between the two extraction protocols at $p < 0.05$.

https://doi.org/10.1021/acsomega.3c01370
ACS Omega 2023, 8, 20755−20766

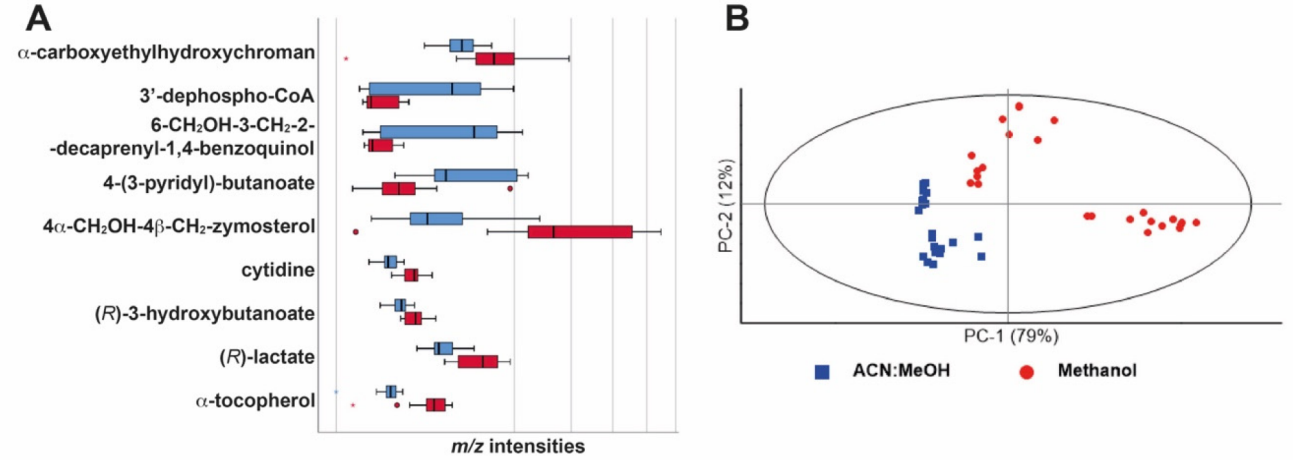

Figure 1. (A) Nine metabolites significantly different between the two extraction protocols ($p < 0.001$) and (B) the corresponding PCA score-plot of the most intense m/z peaks for the four patients' samples.

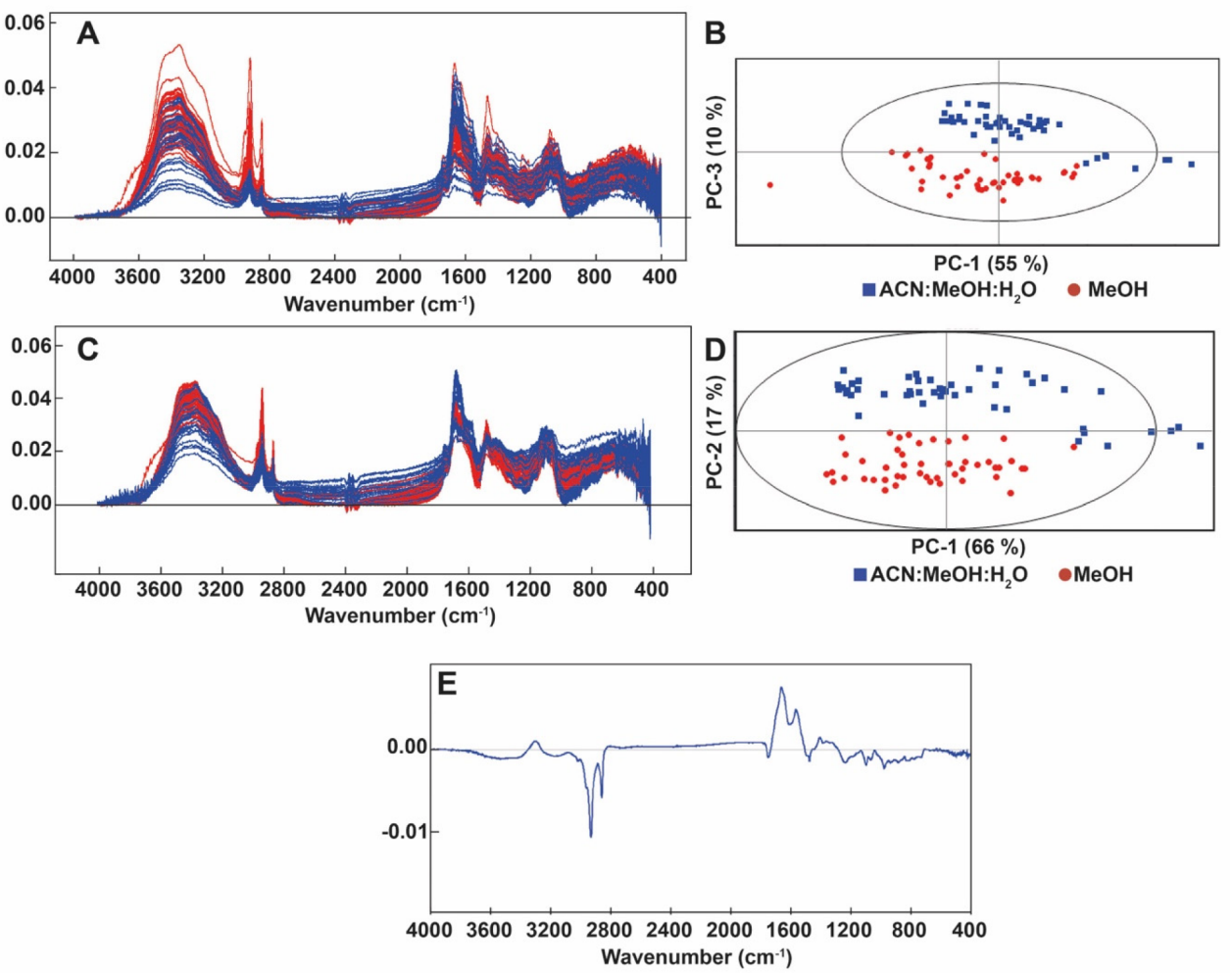

Figure 2. (A and C) FTIR spectra obtained from the two extraction protocols for four patient samples and (B and D) corresponding PCA based on spectra with (A and B) atmospheric and baseline corrections and (C and D) atmospheric and baseline corrections and unit vector normalization. PCA is presented with Hotelling's T^2 ellipse at 5% significance. (E) Representation of the PC2 loading vector from panel D.

ences in elution settings and other UPLC-MS/MS system characteristics.

Considering both RP and HILIC systems, a very similar number of features was obtained with both extraction protocols, i.e., 1882 with MeOH and 2022 with the ACN/MeOH protocol, in constrast to other authors' observations, where the methanol-based extractions present a higher coverage of metabolites than the obtained with ACN.[5] This discrepancy can be from using, in the present work, a mixture

https://doi.org/10.1021/acsomega.3c01370
ACS Omega 2023, 8, 20755−20766

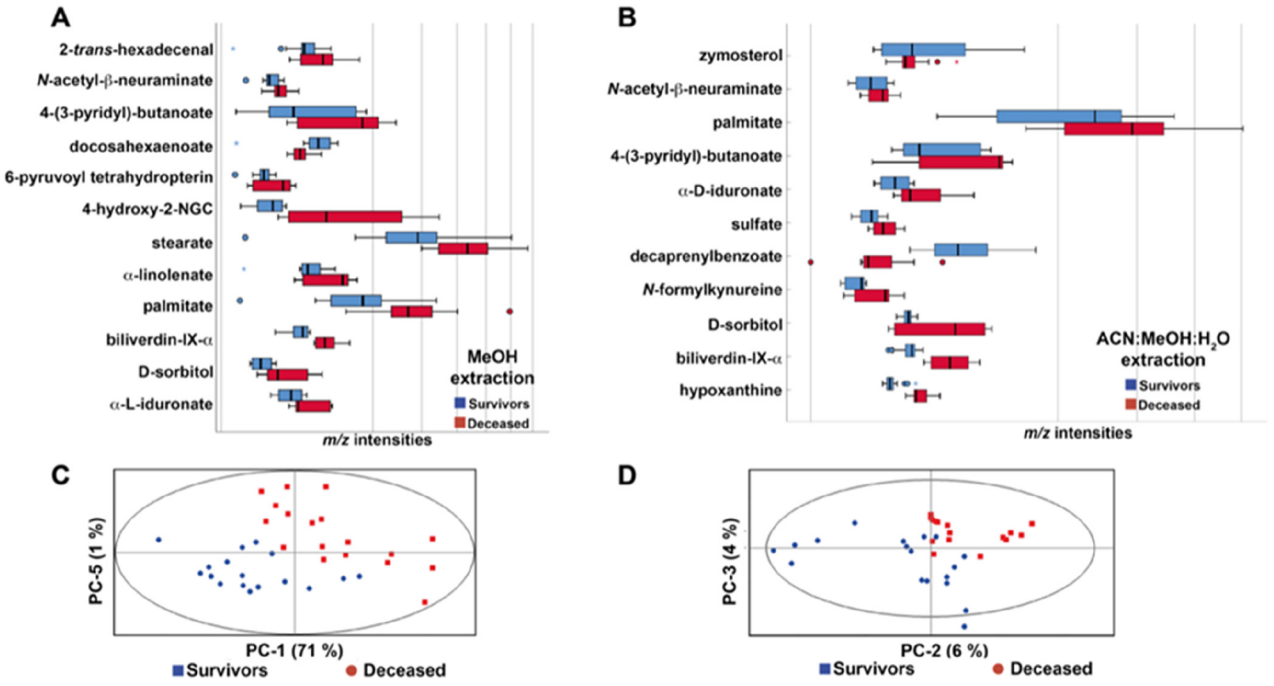

Figure 3. Metabolites differently present between samples of deceased and surviving patients ($p < 0.05$), analyzed by RP-UPLC-MS/MS and according to the metabolome extraction with (A and C) MeOH or (B and D) ACN/MeOH and the corresponding PCA considering the most intense m/z peaks of these metabolites.

of solvents, i.e., ACN/MeOH, and not only ACN, indicating the advantage of using the solvent mixture.

From all features, 925 were detected as being distinct between the two extractions protocols at $p < 0.05$ (Table 1), pointing out the complementarity between the two protocols. The corresponding metabolites for the nine features significantly different between the protocols, at $p < 0.001$, were identified (Figure. 1A). The PCA of the most intense m/z peak from these nine metabolites, as expected, places scores from the MeOH protocol in a different region than those obtained from the ACN/MeOH protocol (Figure. 1B).

From the nine metabolites, seven were hydrophobic, and the following six were present in higher quantities in samples extracted with MeOH: the hydrophilic metabolite lactate (2.0-fold higher), cytidine (2.5-fold higher), the small hydrophobic molecule α-tocopherol (4.1-fold higher) and its degradation metabolite α-carboxyethyl-hydroxychroman (2.1-fold higher), the short-chain fatty acid anion 3-hydroxybutanoate (1.7-fold higher), and the intermediate from cholesterol biosynthesis 4α-CH_2OH-4β-CH_2-zymosterol (6.9-fold higher). In contrary, the following hydrophobic metabolites were present in higher quantities in samples extracted with ACN/MeOH: pyridine 4-(3-pyridyl)-butanoate (5.5-fold higher), hydroquinone 6-CH_2OH-3-CH_2-2-decaprenyl-1,4-benzoquinol (11.8-fold higher), and the intermediate metabolite in pantothenate and coenzyme A (CoA) biosynthesis, 3′-dephospho-CoA (8-fold higher).

Of the nine metabolites, seven were identified from the RP system. From these, six were detected with the ESI+ mode: α-tocopherol, 4α-hydroxymethyl-4β-methylzymosterol, 4-(3-pyridyl)-butanoate, 6-methoxy-3-methyl-2-all-*trans*-decaprenyl-1,4-benzoquinol, 3′-dephospho-CoA, and α-carboxyethylhydroxychroman. Cytidine was identified with the RP column in the ESI− mode. The remaining two putative molecules, (*R*)-lactate and (*R*)-3-hydroxybutanoate, were obtained through the HILIC column with the ESI− mode. These results are based on HILIC resolving more polar compounds than the RP column and the fact that each chromatographic separation presents different sensitivities and specificities,[31] i.e., the two chromatographic modes complement each other toward a more complete information on the system.

Concerning FTIR-spectral data, it was observed that scores on spectral PCA clustered according to the extraction protocol (Figure 2). This was observed independently of the spectral preprocessing method (Figure 2B versus Figure 2D) and in accordance with that previously observed with the UPLC-MS/MS data. Therefore, FTIR-spectroscopy also detected a different molecular profile of the metabolome according to the extraction protocol.

Normalized spectra minimize the effect of sample quantity in the analysis, reducing the influence of experimental setups. The PC2 based on normalized spectra (Figure 2D) discriminates samples extracted in ACN/MeOH (with positive PC2 values) from samples extracted with MeOH (with negative PC2 values). Therefore, the PC2 loading (Figure 2E) points to the spectral regions that are significantly different between molecules extracted with ACN/MeOH (corresponding to the positive bands) and the molecules extracted with MeOH (corresponding to the negative bands). It was observed that the MeOH-based extraction resulted in molecules richer in functional groups absorbing at wavenumbers 2924 and 2853 cm^{-1}, corresponding to asymmetric and symmetric vibrations of the $-CH_2$ groups from lipids. This is according to the results from UPLC-MS/MS, since from the nine different metabolites obtained between the two extraction protocols the three hydrophobic metabolites existing in higher quantities (zymosterol, α-carboxyethyl-hydroxychroman, and α-tocopherol) were extracted with MeOH. The PC2 loading vector also points out that the extraction protocol with ACN resulted in a higher proportion of molecules with functional groups

https://doi.org/10.1021/acsomega.3c01370
ACS Omega 2023, 8, 20755−20766

Table 2. Distances between Replicated Analyses (n = 6) of Four Patient Samples According to the Extraction Protocol and Based On Nine Metabolites[a]

		MeOH	ACN/MeOH
distances between replicas of a specific sample (mean ± standard deviation)[b]	patient 1	0.2193 ± 0.0718	0.1055 ± 0.0569
	patient 2	0.0966 ± 0.0478	0.0823 ± 0.0353
	patient 5	0.1497 ± 0.0733	0.1222 ± 0.0487
	patient 6	0.3044 ± 0.1642	0.2655 ± 0.1132
quartile distance for replicas of all four samples[b]	median (P25−P75)	0.7195 (0.3075−1.1300)	0.3739 (0.1375−0.5717)
	interquartile range	0.8226	0.4341
	minimum distance	0.0361	0.0205
	maximum distance	1.4760	0.8058
	variance	0.1971	0.0519

[a]As analyzed by UPLC-MS/MS and highlighted in Figure 1. Data are presented as distances between replicas of a specific sample or as distances from replicas of all samples. The most intense m/z peak of each metabolite was considered. [b]Values retrieved from MDS analysis.

Table 3. Distances between Replicated Analyses (n = 12) of Four Patient Samples According to the Extraction Protocol and Based On 140 FTIR Spectral Wavenumbers[a]

		MeOH	ACN/MeOH
distances between replicas of a specific sample (mean ± standard deviation)[b]	patient 1	0.5744 ± 0.5673	0.2833 ± 0.1652
	patient 2	0.3471 ± 0.1976	0.2642 ± 0.1688
	patient 5	0.2526 ± 0.1506	0.5482 ± 0.3914
	patient 6	0.4855 ± 0.2532	0.8143 ± 0.5272
quartile distance for replicas of all four samples[b]	median (P25−P75)	0.536 (0.3190−0.8119)	0.5127 (0.2763−0.9426)
	interquartile range	0.4930	0.6663
	minimum distance	0.0091	0.0234
	maximum distance	2.821	3.119
	variance	0.1776	0.2927

[a]As highlighted in Figure 2E. Data are presented as distances between replicas of a specific sample or as distances from replicas of all samples. [b]Values retrieved from MDS analysis.

with bands at 1655 and 1556 cm^{-1}, including vibrations from −C−N groups. This is according to the observation that the compounds existing in a higher proportion when ACN was used were pyridine 4-(3-pyridyl)-butanoate and 3′-dephospho-CoA.

The results obtained from the two platforms (UPLC-MS/MS and FTIR-spectroscopy) are in accordance each other and with other authors pointing that ACN extraction results in more polar metabolites in comparison to MeOH.[17] FTIR spectroscopy outputs were therefore in accordance with UPLC-MS/MS data and other authors, with the advantage of the analysis being much simpler, rapid, and economic in relation to UPLC-MS/MS. Therefore, FTIR spectroscopy can represent a very appealing tool to conduct a qualitative evaluation of sample preparation for metabolomics, as previously also conducted by Kuligowski et al., for example[17]

Reproducibility. The reproducibility associated with each extraction protocol was evaluated, considering UPLC-MS/MS and FTIR-spectroscopy, on the same four patient samples from the previous section (highlighted in bold in Table S1). This was considered per sample, the extraction replicas, and analytical replicas.

For the UPLC-MS/MS analysis, the intensities of the m/z peaks corresponding to the nine metabolites previously identified on the four samples' replicas were represented in the MDS graph (Figure 3). From the duplicate extraction procedures, and triplicate analysis of each extraction, a total of six replicas per sample were considered with exception of two samples due to sample limitation, where for one of the extraction replicas only a unique or duplicate analysis was conducted, respectively.

For each serum sample, the replicas' dispersion was evaluated by determining the distances between them (Figure 3A, Table 2). Independent of the extraction protocol, the samples' dispersion, i.e., reproducibility, depended on the sample. For both extraction protocols, in mean terms, the sample dispersion varied threefold from the less disperse sample to the ones with higher dispersion (Table 2). It was observed that serum samples extracted with MeOH presented higher distances between replicas (with a median of 0.72) in comparison to the ones obtained with ACN/MeOH (with a median of 0.37) (Figure S1A, Table 2). Therefore, the extraction protocol with only MeOH, in median terms, results in 1.9-fold lower reproducibility/precision in relation to the extraction protocol with ACN. This is not in accordance with other authors' observations, pointing that an extraction based on MeOH usually leads to more reproducible results.[19] However, these authors did not evaluate mixtures of solvents, such as the one used in the present work with ACN/MeOH. Additionally, the outputs can depend on a sample's characteristic, i.e., from the patient's physiological state. In the present study, all patients were critically ill, as all were at the ICU, and were submitted to mechanical ventilation and extracorporeal membrane oxygenation (ECMO), where 3 out of 4 of these patients died in the first two weeks after sample harvesting. This hypothesis is in accordance with the replica dispersion depending on the patient (Figure S1, Table 2). It is worth pointing out that extraction based on MeOH resulted in higher replica dispersion, i.e., in less precise measurements, but also in a higher distance between samples from different patients, which can result in higher sensitivities. Therefore, the higher replica dispersion obtained from this protocol does not

https://doi.org/10.1021/acsomega.3c01370
ACS Omega 2023, 8, 20755−20766

Table 4. Metabolites Differently Present between Deceased and Survivor Patients as Detected by RP-UPLC-MS/MS According to the Metabolome Extraction Protocol[a]

MeOH extraction			ACN/MeOH extraction		
metabolite	m/z	fold change[b]	metabolite	m/z	fold change[b]
α-L-iduronate	193.04	1.78 ↑ **	α-L-iduronate	193.04	2.18 ↑ **
D-sorbitol	181.07	3.26 ↑ **	D-sorbitol	183.08	2.65 ↑ ***
N-acetyl-β-neuraminate	310.12	1.45 ↑ **	*N*-acetyl-β-neuraminate	310.12	1.46 ↑ *
biliverdin-IX-α	583.26	2.10 ↑ ***	biliverdin-IX-α	583.26	2.37 ↑ ***
4-(3-pyridyl)-butanoate	166.09	2.17 ↑ **	4-(3-pyridyl)-butanoate	166.09	1.90 ↑ **
palmitate	257.25	2.23 ↑ ***	palmitate	257.25	1.55 ↑ *
α-linolenate	279.23	1.78 ↑ **	3,4-dihydroxy-5-all-*trans*-decaprenylbenzoate	835.67	3.12 ↓ **
stearate	285.28	1.66 ↑ **	4α-OCH3-4β-CH-5α-zymosterol	429.37	2.04 ↓ *
2-*trans*-hexadecenal	239.24	1.58 ↑ **			
(4Z,7Z,10Z,13Z,16Z,19Z)-docosahexaenoate	329.24	1.58 ↓ **	hypoxanthine	135.03	2.04 ↑ ***
4-hydroxy-2-nonenal-glutathione conjugate	465.21	12.12 ↑ **	*N*-formylkynurenine	238.09	2.85 ↑ ***
6-pyruvoyl tetrahydropterin	238.09	2.24 ↑ **	sulfate	96.96	1.59 ↑ **

[a]The most intense m/z peak of that metabolite was considered. [b]Change trend compared to samples of survivor patients. ↑, up-regulated. ↓, down-regulated. *, $p < 0.05$; **, $p < 0.01$; ***, $p < 0.001$.

necessary imply that this extraction method will lead to worse prediction models of a target pathophysiological state.

Comparing the dispersion of duplicates of extractions with the dispersion of triplicates of analysis per extraction (Figure S1B), it was observed that, in general, triplicates of analysis per extraction are closer together compared to the other extraction replica. Consequently, the extraction procedure presents a higher variability than the UPLC-MS/MS analysis. A consequence of this is, for example, seen for MeOH extraction, where the second replica of extraction of sample 2 is closer to replicas of sample 1. This can impair the analysis sensitivity and specificity.

Concerning FTIR-spectral data, the PCA based on spectral regions that were highlighted in the PC2 loading vector in Figure 2E presenting values below −0.04 or higher to 0.04 was considered. This spectral region corresponded to 140 wavenumbers. It considered 12 replicas per sample, resulting from triplicates of each extraction protocol, followed by quadruplicate FTIR spectroscopic analysis per extraction. It was observed that the dispersion between the 12 replicated analyses of the four samples in the PCA score-plot depended on the sample (Figure S2, Table 3), as previously observed with the UPLC-MS/MS analysis. For both extraction protocols, the sample dispersion, as obtained from the spectral data, varied between 2.3- and 2.9-fold considering the extractions without and with ACN, respectively. In contrast to what was observed with UPLC-MS/MS analysis, the dispersion of FTIR spectral data was identical for both extraction techniques (0.54 and 0.51 for samples extracted with MeOH and ACN/MeOH, respectively). This can be due to FTIR spectroscopy's lower sensitivity in relation to UPLC-MS/MS and/or due to the much higher variance associated with FTIR spectroscopy, since a much higher number of variables are used in the PCA (i.e., of 140 wavenumbers) in relation to the PCA based on UPLC-MS/MS data that considered nine m/z peaks.

In contrast to what was observed with UPLC-MS/MS, where different patients' samples were more separated between each other when extracted in MeOH, the spectral PCA did not show any effect of the extraction protocol on distances between different samples, again probably due to the low sensitivity of FTIR spectroscopy and/or the higher number of variables used in this analysis in relation to UPLC-MS/MS.

Comparing the dispersion of triplicates of the extraction protocol with the quadruplicate replicas of analysis per extraction by FTIR-spectroscopy, it was also observed that the extraction replica has a higher impact than the replicate analysis of each extraction on scores, as the replicate analysis of each extraction tends to be grouped and more separate than other extractions replicas. This was according to the UPLC-MS/MS analyses, even though in spectral PCA the distances between samples are not as high as those observed in the MS peak PCA.

Prediction of Patient Outcomes. The serum metabolome of the two extraction protocols was used to predict the outcomes of six patients hospitalized in the ICU (Table S1). The metabolome analyzed by RP-UPLC-MS/MS was considered due to the significantly higher number of features obtained with this system in comparison to the HILIC-based system (Table 1). The metabolome fingerprint obtained by FTIR-spectroscopy was also considered. All patients were diagnosed with COVID-19. Due to the severity of their symptoms, all patients were under mechanical ventilation and extracorporeal membrane oxygenation (Table S1). Of these six patients, three died in the ICU. From data of UPLC-MS/MS, 17 different metabolites were identified as significantly different ($p < 0.05$) between samples of deceased and surviving patients (Table 4, Figure 3). Of these 17 metabolites, only 6 were simultaneously identified by both extraction protocols, where further 6 and 5 were specifically identified by the MeOH and the ACN/MeOH extraction protocols, respectively. This points to the complementary of the extraction protocols.

From the MeOH protocol, 10 metabolites were reported in the ESI+ operation mode and 2 in the ESI− mode. For the ACN protocol, 8 metabolites were identified in ESI+ and 3 in ESI− from the RP column. Most of the metabolites were up-regulated in deceased patients' samples with the exception of (4Z,7Z,10Z,13Z,16Z,19Z)-docosahexaenoate, 3,4-dihydroxy-5-all-*trans*-decaprenylbenzoate, and 4α-OCH_3-4β-CH-5α-zymosterol, which were up-regulated in the surviving patients.

From the metabolites up-regulated in deceased patients, most of them are associated with oxidative and inflammatory processes. Lipid peroxidation products such as 4-hydroxynonenal are indicative of oxidative stress. Biliverdin is a product of heme degradation,[33] and its up-regulation can be indicative of liver impairment or hemolysis and of excess bilirubin

https://doi.org/10.1021/acsomega.3c01370
ACS Omega 2023, 8, 20755−20766

concentration. Bilirubin acts as a reducing agent upon oxidative damage, being converted to biliverdin-IX-α. Thus, higher levels of this metabolite can be associated with oxidative damage.[34,35] Furthermore, SARS-CoV-2 is able to recruit biliverdin at the level of the spike protein via allostery, dampening the binding with neutralizing antibodies and leading to the worsening of the clinical condition of COVID-19 patients.[36] Increase in the level of palmitic acid has been correlated with inflammatory mediation and increased apoptotic events, being associated with worse outcomes in COVID-19 patients.[37] Higher levels of 4-hydroxy-2-nonenal-glutathione in deceased patients may indicate enhanced levels of reactive oxygen species (ROS). Sulfate (SO_3^-) and iduronic acid (IdoA) may partially result from the glycosaminoglycan dermatan sulfate degradation, which has been associated with the SARS-CoV-2 infection[38] both through the virus' direct effect on tissues and indirectly through inflammatory processes. Hypoxanthine is associated with the purine deoxyribonucleoside metabolism, and its up-regulation has been associated with extracellular extravasation of the molecular precursor ATP due to cellular damage during viral sequestering from SARS-CoV-2 in pneumocytes. Thus, it has been considered an indicator of inflammation and hypoxia.[39,40] *N*-Formyl kynurenine results from tryptophan metabolism by the enzymes indoleamine 2,3-dioxygenase and tryptophan 2,3-dioxygenase, which can be induced by an inflammatory environment,[41] and has been associated with a poor prognosis in COVID-19 patients.[42,43]

The following metabolites were also up-regulated in deceased patients: 2-*trans*-Hexadecenal is an intermediary byproduct of sphingosine and sphingosine-1-phosphate metabolism that is involved in the beta-oxidation pathway and apoptosis.[44] 6-Pyruvoyl tetrahydropterin is an intermediate metabolite from tetrahydrobiopterin de novo biosynthesis. Sorbitol can be an indication of energetic catabolism dysregulation, for when hexokinase activity is decreased/impaired the glucose−sorbitol pathway is preferred.[45] Sorbitol's effects include diuretic, laxative, and cathartic properties. High levels of *N*-acetyl-β-neuraminate, from glycoproteins/lipids and polysaccharides, in urine and serum can be indicative of renal failure.[46] The pyridine derivate, 4-(3-pyridyl)-butanoate, is associated with the nicotine degradation pathway.[47]

Concerning the down-regulated metabolites in deceased patients, the ubiquinol precursor, 3,4-dihydroxy-5-all-*trans*-decaprenylbenzoate, is involved in the mechanism of the regeneration of coenzyme Q10, which is responsible for the reduction and neutralization of free radicals and ROS and increasing the efficiency of electron transport on the mitochondria. Depletion of this molecule, evident on deceased patients, is indicative of oxidative damage, energetic catabolism dysregulation, and even apoptotic events.[48,49] This can be related to the high expression of hypoxanthine and biliverdin, as less 3,4-dihydroxy-5-all-*trans*-decaprenylbenzoate is available due to presence of oxidative species. 4α-OCH_3-4β-CH-5α-Zymosterol takes part in the zymosterol biosynthesis pathway. It is a precursor to zymosterone that ultimately enters in cholesterol biosynthesis. Studies have correlated higher cholesterol bioavailability with higher efficacy of SARS-CoV-2 cell entry by lipidic rafts present at the cell membrane.[50] At the same time, dysregulation of the cholesterol pathway leads to an augmentation of the level of these lipids in the bloodstream, promoting the inflammatory status/cytokine storm.[51] Finally, (4*Z*,7*Z*,10*Z*,13*Z*,16*Z*,19*Z*)-docosahexaenoate is a PUFA anion that takes part in the resolvin D biosynthesis. It contributes to the decline in pro-inflammatory mediator production, which decreases lung neutrophil recruitment, IL-6 production, and apoptosis by macrophages, attenuating COVID-19's complications.[52]

Focusing on the search for biomarkers of the patient's outcome, the PCA of the most intense m/z peaks of the metabolite sets highlighted in Table 4 points to the possibility of predicting the patient prognosis, since scores from deceased patients are located on a different region of the score-plot (Figure 3B and D). A LDA of the most intense m/z of this metabolites set was trained with samples from four patients, randomly selected, resulting in an accuracy of 100% to predict the patients' outcome independent of the extraction protocol (Table 5). The samples were selected randomly as follows: two patient samples were randomly selected out of the three patients that did not die, and two patient samples were randomly selected out of the three patients that died. These models were subsequently tested with samples from the patients that were not used for model training (Table 5). The independent validation data set resulted in excellent accuracies (>90%), sensitivities (>80%), and specificities (>100%) in the prediction of a patient's death in the ICU. Slightly better models were obtained with the solvent mixture containing ACN, leading to an accuracy, specificity, and sensitivity of 100%.

Table 5. LDA Model Performance for the Training (n = 4 patients) and Independent Test (n = 2 patients) Data Sets Based on Metabolites Analyzed by RP-UPLC-MS/MS According to the Metabolome Extraction Protocol[a]

	extraction with MeOH		extraction with ACN/MeOH	
	predicted		predicted	
model performance	training set	test set	training set	test set
accuracy	100%	90%	100%	100%
sensitivity (recall)	100%	80%	100%	100%
specificity	100%	100%	100%	100%
precision	100%	100%	100%	100%
F1	100%	90%	100%	100%

[a]Note: Deceased patients' samples were considered positive outputs, whereas survivors' ones were considered negative outputs.

PCA of the FTIR-spectra also points to the possibility of predicting the patients' outcome, as data from surviving patients are in a distinct region of the score-plot (Figure 4). PCA-LDA models were built based on FTIR-spectra between 800 to 4000 cm^{-1} (Figure 4, Table 6). The region between 400 and 800 cm^{-1} presents spectral noise and was consequently eliminated to improve the performance of the PCA-LDA models (data not shown). Excellent PCA-LDA models were obtained based on both extraction protocols, where the one with ACN/MeOH presented slight better performance (Table 6), as previously observed with UPLC-MS/MS data.

Overall, data obtained from both RP-UPLC-MS/MS and FTIR spectroscopy enabled the devlopment of excellent discriminant analysis models that, based on an independent validation data set, led to predictions of ≥90% accuracy, specificity, and sensitivity. Despite all this, it is worth highlighting the high limitations of the models due to the low number of samples.

https://doi.org/10.1021/acsomega.3c01370
ACS Omega 2023, 8, 20755−20766

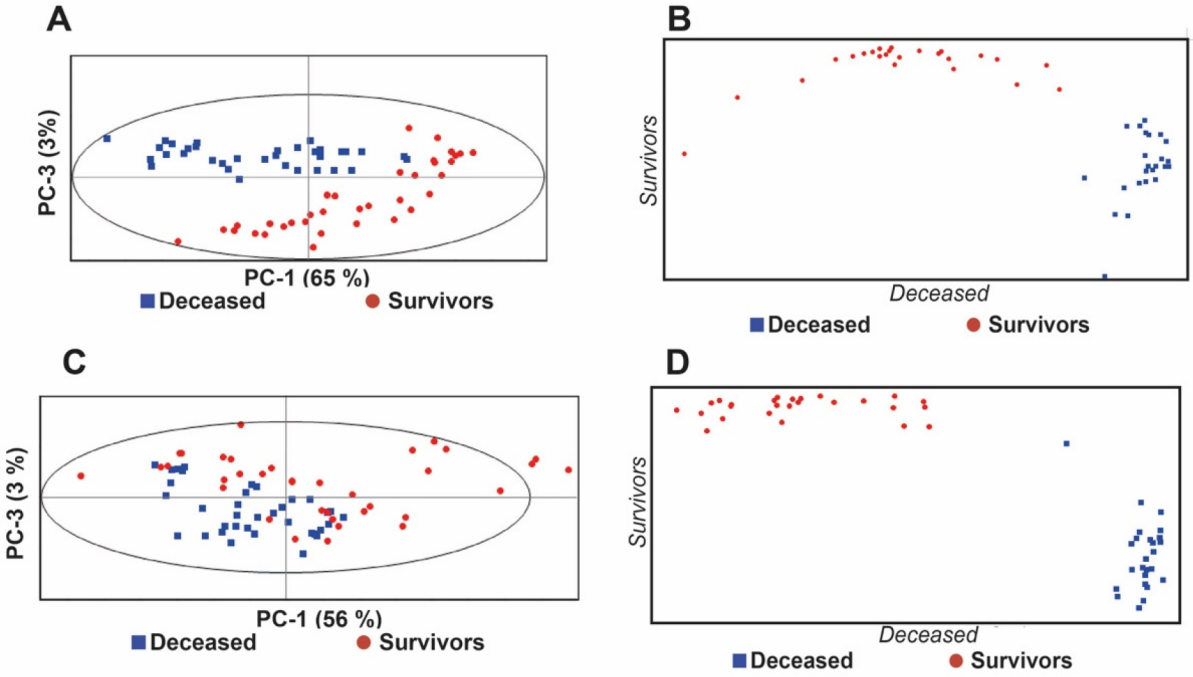

Figure 4. (A and C) PCA of FTIR spectra preprocessed by atmospheric and baseline corrections from the four patient samples and (B and D) corresponding PCA-LDA models according to the extraction protocol based on (A and B) MeOH or (C and D) ACN/MeOH. PCA-LDA (B and D) displayed an accuracy of 100% using two categories and the linear method, with seven projected components.

Table 6. PCA-LDA Model Performance for the Training (n = 4 patients) and Independent Test (n = 2 patients) Data Sets Based On FTIR Spectra Preprocessed by Atmospheric and Baseline Corrections According to the Metabolome Extraction Protocol[a]

	extraction with MeOH		extraction with ACN/MeOH	
	predicted		predicted	
model performance	training set	test set	training set	test set
accuracy	100%	95%	100%	100%
sensitivity (recall)	100%	100%	100%	100%
specificity	100%	90%	100%	100%
precision	100%	92%	100%	100%
F1	100%	96%	100%	100%

[a]Note: Deceased patients' samples were considered positive outputs, whereas survivors' ones were considered negative outputs.

DISCUSSION

Metabolomics is a very appealing tool to discover biomarkers from biofluids such as serum. However, due to the highly complex analytical process, there are diverse variables that impact the study output, including the metabolome isolation method and the main analytical technique used to characterize it. In the present work, the impact of two protocols to obtain the serum metabolome, one using MeOH and another using a mixture of MeOH and ACN, on the metabolome analyses was evaluated by UPLC-MS/MS, including an RP and HILIC system, and FTIR-spectroscopy.

Both extraction protocols resulted in similar numbers of total features obtained in UPLC-MS/MS (1882 and 2022 m/z peaks with the MeOH and ACN/MeOH, respectively), where a high proportion of them (925 features) were distinct between the two extraction protocols ($p < 0.05$). This highlights that both extraction protocols are complementary. Despite this, most (i.e., 67%) of the metabolites differently extracted with the two protocols ($p < 0.001$) were present in higher quantities in the MeOH-extracted samples.

It was observed that replicas of metabolome extractions were less reproducible than replicas of the UPLC-MS/MS analysis. It was also observed that the reproducibility was affected by the sample composition and that the MeOH led to, in mean terms, 1.9-fold less reproducible analysis but a higher difference between samples of different patients. That is, MeOH extractions resulted in less precise but potentially more sensitive measurements.

To better evaluate the real impact of the extraction protocol, the protocols were also compared to predict patient's outcome, concerning mortality of critically ill COVID-19 patients hospitalized at ICU. To achieve that, a LDA-PCA model was built on data from six patients, where three died in the ICU. It was considered the metabolites differently present between deceased and surviving patients ($p < 0.05$) detected by RP-UPLC-MS/MS. For this study, only data from the RP-based system was used, since the RP-column leaded to 4.2- to 5-fold higher number of features in comparison to the HILIC. Indeed, from the significantly different metabolites detected with both extraction protocols ($p < 0.001$), the majority (77%) were detected with the RP-based system. Very good mortality prediction models were achieved with both extraction protocols, with the MeOH- and ACN/MeOH-based protocols resulting in accuracies of 90% and 100%, respectively. Despite the limitation of the study, based on a low number of patients ($n = 6$), this result is in accordance with the MeOH extraction being the less precise, and most of the metabolites identified as deregulated in critically ill patients were in accordance with the literature.

The effect of the extraction protocol was also evaluated by the metabolome analysis by FTIR spectroscopy which, despite

https://doi.org/10.1021/acsomega.3c01370
ACS Omega 2023, 8, 20755−20766

not identifying metabolites, has been applied in previous studies to acquire the metabolome molecular fingerprint in a rapid, economic, and simple but also sensitive and specific mode. Indeed, the main observations demonstrated previously with the UPLC-MS/MS based platform were also observed with the FTIR-spectroscopy. For example, different molecular profiles were also detected between the two extraction protocols, where samples extracted with MeOH presented a significant higher proportion of lipidic molecules, according to the observation by UPLC-MS/MS that the three hydrophobic metabolites existing in higher quantities were also observed in MeOH-extracted samples. It was also observed by FTIR spectroscopy that the ACN/MeOH-extracted samples were richer in CN groups, according to the observation with UPLC-MS/MS that pyridine 4-(3-pyridyl)-butanoate and 3′-dephospho-CoA were present in higher proportions in samples with this extraction protocol. According to UPLC-MS/MS analysis, it was also observed with FTIR spectroscopy that replicas of extractions were less reproducible than replicas of the analysis and that reproducibility depended on the sample composition. However, in contrast to the UPLC-MS/MS platform, the reproducibility observed with the MeOH-extracted samples was similar to the ACN/MeOH-extracted samples, most probably due to the lower sensitivity and/or due to the higher number of variables used with FTIR spectral data. Despite this, excellent PCA-LDA models were obtained with FTIR spectroscopy with accuracies >95% for both extraction protocols, achieving 100% accuracy with ACN/MeOH, as observed with the UPLC-MS/MS system.

Therefore, FTIR spectroscopy can represent an excellent tool to optimize extraction protocols and even to develop models to predict target phenotypes, in this case to predict mortality in critically ill patients. Advantages of FTIR spectroscopy include its simplicity of analysis, the high-throughput analysis, enabling, for example, the simultaneous analysis of hundreds of microliter volumes of samples (from for example 5 to 25 μL), more economic and rapid while leading to predicting models as accurate as those obtained by the UPLC-MS/MS platform. Therefore, FTIR spectroscopy represents a very interesting complementary technique for metabolome characterization. The advantages of the UPLC-MS/MS platform are the identification of associated metabolites, which can facilitate biomarker validation and acceptance by the community. Furthermore, the identification of metabolites also helps to identify deregulated metabolic pathways and consequently the understanding of the underlying pathophysiological mechanisms, which can be used to improve therapies and even to discover new therapies.

■ ASSOCIATED CONTENT

Supporting Information

The Supporting Information is available free of charge at https://pubs.acs.org/doi/10.1021/acsomega.3c01370.

Detailed demographic data from patients, detailed XCMS parameters for metabolomics analysis, and multidimensional scaling (MDS) results (PDF)

■ AUTHOR INFORMATION

Corresponding Author

Cecília R. C. Calado − *Instituto Superior de Engenharia de Lisboa (ISEL), Instituto Politécnico de Lisboa, 1959-007 Lisboa, Portugal; Centro de Investigação em Modelação e Optimização de Sistemas Multifuncionais (CIMOSM), Instituto Superior de Engenharia de Lisboa (ISEL), Instituto Politécnico de Lisboa, 1959-007 Lisboa, Portugal*; Email: cecilia.calado@isel.pt

Authors

Tiago A. H. Fonseca − *Instituto Superior de Engenharia de Lisboa (ISEL), Instituto Politécnico de Lisboa, 1959-007 Lisboa, Portugal*; orcid.org/0000-0003-0741-2211

Cristiana P. Von Rekowski − *Instituto Superior de Engenharia de Lisboa (ISEL), Instituto Politécnico de Lisboa, 1959-007 Lisboa, Portugal*; orcid.org/0009-0009-6843-1935

Rúben Araújo − *Instituto Superior de Engenharia de Lisboa (ISEL), Instituto Politécnico de Lisboa, 1959-007 Lisboa, Portugal*

M. Conceição Oliveira − *Centro de Química Estrutural, Institute of Molecular Sciences, Instituto Superior Técnico, Universidade de Lisboa, 1049-001 Lisboa, Portugal*

Gonçalo C. Justino − *Centro de Química Estrutural, Institute of Molecular Sciences, Instituto Superior Técnico, Universidade de Lisboa, 1049-001 Lisboa, Portugal*; orcid.org/0000-0003-4828-4738

Luís Bento − *Intensive Care Department, Centro Hospitalar Universitário de Lisboa Central (CHULC), 1150-199 Lisboa, Portugal; Integrated Pathophysiological Mechanisms, CHRC, NOVA Medical School, Faculdade de Ciências Médicas, NMS, FCM, Universidade NOVA de Lisboa, 1169-056 Lisboa, Portugal*; orcid.org/0000-0002-0260-003X

Complete contact information is available at: https://pubs.acs.org/10.1021/acsomega.3c01370

Author Contributions

Conceptualization, T.F., C.C., and G.J.; methodology, T.F., C.C., and G.J.; formal analysis, T.F., C.R.,R.A., G.J., and C.C.; original draft preparation, T.F., G.J., and C.C.; and writing and review, all authors. All authors have read and agreed to the published version of the manuscript.

Funding

This research was funded by Fundação para a Ciência e a Tecnologia (FCT), Grants DSAIPA/DS/0117/2020 and RNEM-LISBOA-01-0145-FEDER-022125 (Portuguese Mass Spectrometry Network). The Centro de Quimica Estrutural is a Research Unit funded by FCT through projects UIDB/00100/2020 and UIDP/00100/2020. The Institute of Molecular Sciences is an Associate Laboratory funded by FCT through project LA/P/0056/2020.

Notes

The authors declare no competing financial interest.

■ ACKNOWLEDGMENTS

Special thanks to Professor Doctor Ana Martins for the kind help with the multidimension scaling analysis.

■ REFERENCES

(1) Wishart, D. S. Metabolomics for Investigating Physiological and Pathophysiological Processes. *Physiol. Rev.* **2019**, *99* (4), 1819−1875.

(2) Ellis, D. I.; Dunn, W. B.; Griffin, J. L.; Allwood, J. W.; Goodacre, R. Metabolic Fingerprinting as a Diagnostic Tool. *Pharmacogenomics* **2007**, *8* (9), 1243−1266.

(3) Muthubharathi, B. C.; Gowripriya, T.; Balamurugan, K. Metabolomics: Small Molecules That Matter More. *Mol. Omi.* **2021**, *17* (2), 210−229.

(4) Wishart, D. S.; Guo, A. C.; Oler, E.; Wang, F.; Anjum, A.; Peters, H.; Dizon, R.; Sayeeda, Z.; Tian, S.; Lee, B. L.; Berjanskii, M.; Mah, R.; Yamamoto, M.; Jovel, J.; Torres-Calzada, C.; Hiebert-Giesbrecht, M.; Lui, V. W.; Varshavi, D.; Varshavi, D.; Allen, D.; Arndt, D.; Khetarpal, N.; Sivakumaran, A.; Harford, K.; Sanford, S.; Yee, K.; Cao, X.; Budinski, Z.; Liigand, J.; Zhang, L.; Zheng, J.; Mandal, R.; Karu, N.; Dambrova, M.; Schiöth, H. B.; Greiner, R.; Gautam, V. HMDB 5.0: The Human Metabolome Database for 2022. *Nucleic Acids Res.* **2022**, *50* (D1), D622.
(5) Martias, C.; Baroukh, N.; Mavel, S.; Blasco, H.; Lefèvre, A.; Roch, L.; Montigny, F.; Gatien, J.; Schibler, L.; Dufour-Rainfray, D.; Nadal-Desbarats, L.; Emond, P. Optimization of Sample Preparation for Metabolomics Exploration of Urine, Feces, Blood and Saliva in Humans Using Combined NMR and UHPLC-HRMS Platforms. *Molecules* **2021**, *26* (14), 4111.
(6) Jacob, M.; Lopata, A. L.; Dasouki, M.; Abdel Rahman, A. M. Metabolomics toward Personalized Medicine. *Mass Spectrom. Rev.* **2019**, *38* (3), 221−238.
(7) Li, X.; Fan, X.; Yang, H.; Liu, Y. Review of Metabolomics-Based Biomarker Research for Parkinson's Disease. *Mol. Neurobiol.* **2022**, *59* (2), 1041−1057.
(8) Lotta, L. A.; Scott, R. A.; Sharp, S. J.; Burgess, S.; Luan, J.; Tillin, T.; Schmidt, A. F.; Imamura, F.; Stewart, I. D.; Perry, J. R. B.; Marney, L.; Koulman, A.; Karoly, E. D.; Forouhi, N. G.; Sjögren, R. J. O.; Näslund, E.; Zierath, J. R.; Krook, A.; Savage, D. B.; Griffin, J. L.; Chaturvedi, N.; Hingorani, A. D.; Khaw, K.-T.; Barroso, I.; McCarthy, M. I.; O'Rahilly, S.; Wareham, N. J.; Langenberg, C. Genetic Predisposition to an Impaired Metabolism of the Branched-Chain Amino Acids and Risk of Type 2 Diabetes: A Mendelian Randomisation Analysis. *PLOS Med.* **2016**, *13* (11), No. e1002179.
(9) Hrydziuszko, O.; Perera, M. T. P. R.; Laing, R.; Kirwan, J.; Silva, M. A.; Richards, D. A.; Murphy, N.; Mirza, D. F.; Viant, M. R. Mass Spectrometry Based Metabolomics Comparison of Liver Grafts from Donors after Circulatory Death (DCD) and Donors after Brain Death (DBD) Used in Human Orthotopic Liver Transplantation. *PLoS One* **2016**, *11* (11), No. e0165884.
(10) Araújo, R.; Bento, L. F. N.; Fonseca, T. A. H.; Von Rekowski, C. P.; da Cunha, B. R.; Calado, C. R. C. Infection Biomarkers Based on Metabolomics. *Metabolites* **2022**, *12* (2), 92.
(11) Dunn, W. B.; Broadhurst, D.; Begley, P.; Zelena, E.; Francis-McIntyre, S.; Anderson, N.; Brown, M.; Knowles, J. D.; Halsall, A.; Haselden, J. N.; Nicholls, A. W.; Wilson, I. D.; Kell, D. B.; Goodacre, R. Procedures for Large-Scale Metabolic Profiling of Serum and Plasma Using Gas Chromatography and Liquid Chromatography Coupled to Mass Spectrometry. *Nat. Protoc.* **2011**, *6* (7), 1060−1083.
(12) Pommié, C.; Levadoux, S.; Sabatier, R.; Lefranc, G.; Lefranc, M.-P. IMGT Standardized Criteria for Statistical Analysis of Immunoglobulin V-REGION Amino Acid Properties. *J. Mol. Recognit.* **2004**, *17* (1), 17−32.
(13) Baker, M. J.; Trevisan, J.; Bassan, P.; Bhargava, R.; Butler, H. J.; Dorling, K. M.; Fielden, P. R.; Fogarty, S. W.; Fullwood, N. J.; Heys, K. A.; Hughes, C.; Lasch, P.; Martin-Hirsch, P. L.; Obinaju, B.; Sockalingum, G. D.; Sulé-Suso, J.; Strong, R. J.; Walsh, M. J.; Wood, B. R.; Gardner, P.; Martin, F. L. Using Fourier Transform IR Spectroscopy to Analyze Biological Materials. *Nat. Protoc.* **2014**, *9* (8), 1771−1791.
(14) Sales, K. C.; Rosa, F.; Sampaio, P. N.; Fonseca, L. P.; Lopes, M. B.; Calado, C. R. C. In Situ Near-Infrared (NIR) versus High-Throughput Mid-Infrared (MIR) Spectroscopy to Monitor Biopharmaceutical Production. *Appl. Spectrosc.* **2015**, *69* (6), 760−772.
(15) Sala, A.; Anderson, D. J.; Brennan, P. M.; Butler, H. J.; Cameron, J. M.; Jenkinson, M. D.; Rinaldi, C.; Theakstone, A. G.; Baker, M. J. Biofluid Diagnostics by FTIR Spectroscopy: A Platform Technology for Cancer Detection. *Cancer Lett.* **2020**, *477*, 122−130.
(16) Ribeiro da Cunha, B.; Fonseca, L. P.; Calado, C. R. C. Simultaneous Elucidation of Antibiotic Mechanism of Action and Potency with High-Throughput Fourier-Transform Infrared (FTIR) Spectroscopy and Machine Learning. *Appl. Microbiol. Biotechnol.* **2021**, *105* (3), 1269−1286.
(17) Kuligowski, J.; Pérez-Guaita, D.; Escobar, J.; Lliso, I.; de la Guardia, M.; Lendl, B.; Vento, M.; Quintás, G. Infrared Biospectroscopy for a Fast Qualitative Evaluation of Sample Preparation in Metabolomics. *Talanta* **2014**, *127*, 181−190.
(18) Rico, E.; González, O.; Blanco, M. E.; Alonso, R. M. Evaluation of Human Plasma Sample Preparation Protocols for Untargeted Metabolic Profiles Analyzed by UHPLC-ESI-TOF-MS. *Anal. Bioanal. Chem.* **2014**, *406* (29), 7641−7652.
(19) Want, E. J.; O'Maille, G.; Smith, C. A.; Brandon, T. R.; Uritboonthai, W.; Qin, C.; Trauger, S. A.; Siuzdak, G. Solvent-Dependent Metabolite Distribution, Clustering, and Protein Extraction for Serum Profiling with Mass Spectrometry. *Anal. Chem.* **2006**, *78* (3), 743−752.
(20) Chen, S.; Hoene, M.; Li, J.; Li, Y.; Zhao, X.; Häring, H. U.; Schleicher, E. D.; Weigert, C.; Xu, G.; Lehmann, R. Simultaneous Extraction of Metabolome and Lipidome with Methyl Tert-Butyl Ether from a Single Small Tissue Sample for Ultra-High Performance Liquid Chromatography/Mass Spectrometry. *J. Chromatogr. A* **2013**, *1298*, 9−16.
(21) Yuan, M.; Breitkopf, S. B.; Yang, X.; Asara, J. M. A Positive/Negative Ion−Switching, Targeted Mass Spectrometry−Based Metabolomics Platform for Bodily Fluids, Cells, and Fresh and Fixed Tissue. *Nat. Protoc.* **2012**, *7* (5), 872−881.
(22) A, J.; Trygg, J.; Gullberg, J.; Johansson, A. I.; Jonsson, P.; Antti, H.; Marklund, S. L.; Moritz, T. Extraction and GC/MS Analysis of the Human Blood Plasma Metabolome. *Anal. Chem.* **2005**, *77* (24), 8086−8094.
(23) Roberts, I.; Wright Muelas, M.; Taylor, J. M.; Davison, A. S.; Xu, Y.; Grixti, J. M.; Gotts, N.; Sorokin, A.; Goodacre, R.; Kell, D. B. Untargeted Metabolomics of COVID-19 Patient Serum Reveals Potential Prognostic Markers of Both Severity and Outcome. *Metabolomics* **2022**, *18* (1), 6.
(24) Lu, W.; Su, X.; Klein, M. S.; Lewis, I. A.; Fiehn, O.; Rabinowitz, J. D. Metabolite Measurement: Pitfalls to Avoid and Practices to Follow. *Annu. Rev. Biochem.* **2017**, *86* (1), 277−304.
(25) Chambers, M. C.; Maclean, B.; Burke, R.; Amodei, D.; Ruderman, D. L.; Neumann, S.; Gatto, L.; Fischer, B.; Pratt, B.; Egertson, J.; Hoff, K.; Kessner, D.; Tasman, N.; Shulman, N.; Frewen, B.; Baker, T. A.; Brusniak, M.-Y.; Paulse, C.; Creasy, D.; Flashner, L.; Kani, K.; Moulding, C.; Seymour, S. L.; Nuwaysir, L. M.; Lefebvre, B.; Kuhlmann, F.; Roark, J.; Rainer, P.; Detlev, S.; Hemenway, T.; Huhmer, A.; Langridge, J.; Connolly, B.; Chadick, T.; Holly, K.; Eckels, J.; Deutsch, E. W.; Moritz, R. L.; Katz, J. E.; Agus, D. B.; MacCoss, M.; Tabb, D. L.; Mallick, P. A Cross-Platform Toolkit for Mass Spectrometry and Proteomics. *Nat. Biotechnol.* **2012**, *30* (10), 918−920.
(26) Gowda, H.; Ivanisevic, J.; Johnson, C. H.; Kurczy, M. E.; Benton, H. P.; Rinehart, D.; Nguyen, T.; Ray, J.; Kuehl, J.; Arevalo, B.; Westenskow, P. D.; Wang, J.; Arkin, A. P.; Deutschbauer, A. M.; Patti, G. J.; Siuzdak, G. Interactive XCMS Online: Simplifying Advanced Metabolomic Data Processing and Subsequent Statistical Analyses. *Anal. Chem.* **2014**, *86* (14), 6931−6939.
(27) Zhu, Z.-J.; Schultz, A. W.; Wang, J.; Johnson, C. H.; Yannone, S. M.; Patti, G. J.; Siuzdak, G. Liquid Chromatography Quadrupole Time-of-Flight Mass Spectrometry Characterization of Metabolites Guided by the METLIN Database. *Nat. Protoc.* **2013**, *8* (3), 451−460.
(28) Tautenhahn, R.; Cho, K.; Uritboonthai, W.; Zhu, Z.; Patti, G. J.; Siuzdak, G. An Accelerated Workflow for Untargeted Metabolomics Using the METLIN Database. *Nat. Biotechnol.* **2012**, *30* (9), 826−828.
(29) Tautenhahn, R.; Patti, G. J.; Rinehart, D.; Siuzdak, G. XCMS Online: A Web-Based Platform to Process Untargeted Metabolomic Data. *Anal. Chem.* **2012**, *84* (11), 5035−5039.
(30) Yin, P.; Wan, D.; Zhao, C.; Chen, J.; Zhao, X.; Wang, W.; Lu, X.; Yang, S.; Gu, J.; Xu, G. A Metabonomic Study of Hepatitis B-Induced Liver Cirrhosis and Hepatocellular Carcinoma by Using RP-LC and HILIC Coupled with Mass Spectrometry. *Mol. Biosyst.* **2009**, *5* (8), 868.

https://doi.org/10.1021/acsomega.3c01370
ACS Omega 2023, 8, 20755−20766

(31) Boudah, S.; Olivier, M.-F.; Aros-Calt, S.; Oliveira, L.; Fenaille, F.; Tabet, J.-C.; Junot, C. Annotation of the Human Serum Metabolome by Coupling Three Liquid Chromatography Methods to High-Resolution Mass Spectrometry. *J. Chromatogr. B* **2014**, *966*, 34−47.
(32) Yang, Y.; Cruickshank, C.; Armstrong, M.; Mahaffey, S.; Reisdorph, R.; Reisdorph, N. New Sample Preparation Approach for Mass Spectrometry-Based Profiling of Plasma Results in Improved Coverage of Metabolome. *J. Chromatogr. A* **2013**, *1300*, 217−226.
(33) Wu, B.; Wu, Y.; Tang, W. Heme Catabolic Pathway in Inflammation and Immune Disorders. *Front. Pharmacol.* **2019**, *10* (July), 1−15.
(34) Barañano, D. E.; Rao, M.; Ferris, C. D.; Snyder, S. H. Biliverdin Reductase: A Major Physiologic Cytoprotectant. *Proc. Natl. Acad. Sci. U. S. A.* **2002**, *99* (25), 16093−16098.
(35) Wagener, F. A. D. T. G.; Pickkers, P.; Peterson, S. J.; Immenschuh, S.; Abraham, N. G. Targeting the Heme-Heme Oxygenase System to Prevent Severe Complications Following COVID-19 Infections. *Antioxidants* **2020**, *9* (6), 540.
(36) Rosa, A.; Pye, V. E.; Graham, C.; Muir, L.; Seow, J.; Ng, K. W.; Cook, N. J.; Rees-Spear, C.; Parker, E.; dos Santos, M. S.; Rosadas, C.; Susana, A.; Rhys, H.; Nans, A.; Masino, L.; Roustan, C.; Christodoulou, E.; Ulferts, R.; Wrobel, A. G.; Short, C.-E.; Fertleman, M.; Sanders, R. W.; Heaney, J.; Spyer, M.; Kjær, S.; Riddell, A.; Malim, M. H.; Beale, R.; MacRae, J. I.; Taylor, G. P.; Nastouli, E.; van Gils, M. J.; Rosenthal, P. B.; Pizzato, M.; McClure, M. O.; Tedder, R. S.; Kassiotis, G.; McCoy, L. E.; Doores, K. J.; Cherepanov, P. SARS-CoV-2 Can Recruit a Heme Metabolite to Evade Antibody Immunity. *Sci. Adv.* **2021**, *7* (22), 1−14.
(37) Joshi, C.; Jadeja, V.; Zhou, H. Molecular Mechanisms of Palmitic Acid Augmentation in COVID-19 Pathologies. *Int. J. Mol. Sci.* **2021**, *22* (13), 7127.
(38) Wang, J. Y.; Roehrl, M. W.; Roehrl, V. B.; Roehrl, M. H. A Master Autoantigen-Ome Links Alternative Splicing, Female Predilection, and COVID-19 to Autoimmune Diseases. *J. Transl. Autoimmun.* **2022**, *5*, No. 100147.
(39) Wu, D.; Shu, T.; Yang, X.; Song, J. X.; Zhang, M.; Yao, C.; Liu, W.; Huang, M.; Yu, Y.; Yang, Q.; Zhu, T.; Xu, J.; Mu, J.; Wang, Y.; Wang, H.; Tang, T.; Ren, Y.; Wu, Y.; Lin, S. H.; Qiu, Y.; Zhang, D. Y.; Shang, Y.; Zhou, X. Plasma Metabolomic and Lipidomic Alterations Associated with COVID-19. *Natl. Sci. Rev.* **2020**, *7* (7), 1157−1168.
(40) Doğan, H. O.; Şenol, O.; Bolat, S.; Yıldız, Ş. N.; Büyüktuna, S. A.; Sarıismailoğlu, R.; Doğan, K.; Hasbek, M.; Hekim, S. N. Understanding the Pathophysiological Changes via Untargeted Metabolomics in COVID-19 Patients. *J. Med. Virol.* **2021**, *93* (4), 2340−2349.
(41) Neavin, D.; Liu, D.; Ray, B.; Weinshilboum, R. The Role of the Aryl Hydrocarbon Receptor (AHR) in Immune and Inflammatory Diseases. *Int. J. Mol. Sci.* **2018**, *19* (12), 3851.
(42) Hasan, M. R.; Suleiman, M.; Pérez-López, A. Metabolomics in the Diagnosis and Prognosis of COVID-19. *Front. Genet.* **2021**, *12* (May), No. 721556, DOI: 10.3389/fgene.2021.721556.
(43) Mangge, H.; Herrmann, M.; Meinitzer, A.; Pailer, S.; Curcic, P.; Sloup, Z.; Holter, M.; Prüller, F. Increased Kynurenine Indicates a Fatal Course of Covid-19. *Antioxidants* **2021**, *10* (12), 1960.
(44) Jarugumilli, G. K.; Choi, J. R.; Chan, P.; Yu, M.; Sun, Y.; Chen, B.; Niu, J.; Deran, M.; Zheng, B.; Zoeller, R.; Lin, C.; Wu, X. Chemical Probe to Identify the Cellular Targets of the Reactive Lipid Metabolite 2- Trans-Hexadecenal. *ACS Chem. Biol.* **2018**, *13* (5), 1130−1136.
(45) Maitra, S.; Dutta, D. Downregulation of Hexose Sugar Metabolism in Diabetes Decreases the Rate of Wound Healing. In *Wound Healing, Tissue Repair, and Regeneration in Diabetes*; Bagchi, D., Das, A., Roy, S., Eds.; Elsevier, 2020; pp 259−270. DOI: 10.1016/B978-0-12-816413-6.00013-7.
(46) Kimura, T.; Yasuda, K.; Yamamoto, R.; Soga, T.; Rakugi, H.; Hayashi, T.; Isaka, Y. Identification of Biomarkers for Development of End-Stage Kidney Disease in Chronic Kidney Disease by Metabolomic Profiling. *Sci. Rep.* **2016**, *6* (1), 26138.
(47) Dator, R.; Villalta, P. W.; Thomson, N.; Jensen, J.; Hatsukami, D. K.; Stepanov, I.; Warth, B.; Balbo, S. Metabolomics Profiles of Smokers from Two Ethnic Groups with Differing Lung Cancer Risk. *Chem. Res. Toxicol.* **2020**, *33* (8), 2087−2098.
(48) Ouyang, L.; Gong, J. Mitochondrial-Targeted Ubiquinone: A Potential Treatment for COVID-19. *Med. Hypotheses* **2020**, *144*, No. 110161.
(49) Nelson, D. R.; Hrout, A. Al; Alzahmi, A. S.; Chaiboonchoe, A.; Amin, A.; Salehi-Ashtiani, K. Molecular Mechanisms behind Safranal's Toxicity to HepG2 Cells from Dual Omics. *Antioxidants* **2022**, *11* (6), 1125.
(50) Kočar, E.; Režen, T.; Rozman, D. Cholesterol, Lipoproteins, and COVID-19: Basic Concepts and Clinical Applications. *Biochim. Biophys. Acta* **2021**, *1866*, 158849.
(51) Lee, W.; Ahn, J. H.; Park, H. H.; Kim, H. N.; Kim, H.; Yoo, Y.; Shin, H.; Hong, K. S.; Jang, J. G.; Park, C. G.; Choi, E. Y.; Bae, J.-S.; Seo, Y.-K. COVID-19-Activated SREBP2 Disturbs Cholesterol Biosynthesis and Leads to Cytokine Storm. *Signal Transduct. Target. Ther.* **2020**, *5* (1), 186.
(52) Hathaway, D.; Pandav, K.; Patel, M.; Riva-Moscoso, A.; Singh, B. M.; Patel, A.; Min, Z. C.; Singh-Makkar, S.; Sana, M. K.; Sanchez-Dopazo, R.; Desir, R.; Fahem, M. M. M.; Manella, S.; Rodriguez, I.; Alvarez, A.; Abreu, R. Omega 3 Fatty Acids and COVID-19: A Comprehensive Review. *Infect. Chemother.* **2020**, *52* (4), 478−495.

https://doi.org/10.1021/acsomega.3c01370
ACS Omega 2023, 8, 20755−20766